Structural Plasticity of the Cardiac Nuclear Pore Complex in Response to Regulators of Nuclear Import

Carmen Perez-Terzic, A. Marquis Gacy, Ryan Bortolon, Petras P. Dzeja, Michel Puceat, Marisa Jaconi, Franklyn G. Prendergast, Andre Terzic

Abstract—Communication between the cytoplasm and nucleoplasm of cardiac cells occurs by molecular transport through nuclear pores. In lower eukaryotes, nuclear transport requires the maintenance of cellular energetics and ion homeostasis. Although heart muscle is particularly sensitive to metabolic stress, the regulation of nuclear transport through nuclear pores in cardiomyocytes has not yet been characterized. With the use of laser confocal and atomic force microscopy, we observed nuclear transport in cardiomyocytes and the structure of individual nuclear pores under different cellular conditions. In response to the depletion of Ca^{2+} stores or ATP/GTP pools, the cardiac nuclear pore complex adopted 2 distinct conformations that led to different patterns of nuclear import regulation. Depletion of Ca^{2+} indiscriminately prevented the nuclear import of macromolecules through closure of the nuclear pore opening. Depletion of ATP/GTP only blocked facilitated transport through a simultaneous closure of the pore and relaxation of the entire complex, which allowed other molecules to pass into the nucleus through peripheral routes. The current study of the structural plasticity of the cardiac nuclear pore complex, which was observed in response to changes in cellular conditions, identifies a gating mechanism for molecular translocation across the nuclear envelope of cardiac cells. The cardiac nuclear pore complex serves as a conduit that differentially regulates nuclear transport of macromolecules and provides a mechanism for the control of nucleocytoplasmic communication in cardiac cells, in particular under stress conditions associated with disturbances in cellular bioenergetics and Ca^{2+} homeostasis. **(*Circ Res*. 1999;84:1292-1301.)**

Key Words: nucleus ■ transport ■ Ca^{2+} ■ ATP ■ GTP ■ stress, cellular ■ microscopy

Communication between the cytoplasm and nucleoplasm of eukaryotic cells, including cardiomyocytes, must occur by molecular transport across the nuclear envelope, which separates the 2 compartments.[1–3] Nuclear transport occurs by active or passive mechanisms, depending on the requirements for energy, size of the molecule, and presence of a nuclear localization signal within the molecule to be transported. Although several steps in the transport process have been recognized, including targeting and movement to the nuclear surface, it is translocation through the nuclear envelope that ultimately secures transfer of a molecule between compartments.[3–6] The actual translocation of macromolecules occurs through specialized conduits called nuclear pore complexes (NPCs).[7,8] From studies in *Xenopus* oocytes and yeast, it is known that the NPC is a megadalton complex of heteromultimeric proteins assembled around a central pore that spans both membranes of the nuclear envelope.[7–12] In these less differentiated cell types, NPCs have been described as dynamic complexes, with changes in conformational states observed under different cellular conditions.[13–16] However, in cardiac cells, limited information is available on NPCs,[17] and the regulation of cardiac nuclear transport has not yet been characterized. In particular, it is unknown whether metabolic stress, to which heart muscle displays a high vulnerability, induces conformational changes in NPCs.

Cellular homeostasis requires the maintenance of Ca^{2+} and ATP/GTP pools, which have been implicated in the regulation of nuclear transport in lower eukaryotes.[10,13–16,18,19] In the mammalian cardiomyocyte, depletion of Ca^{2+} or ATP/GTP induced distinct conformational transitions in the NPC, which resulted in differentially regulated nuclear import. In this manner, the cardiac NPC provides a gating mechanism that controls the final step of nuclear transport under specific cellular conditions. Thus, the current study identifies the structural plasticity of the NPC as a critical factor in the response of cardiomyocytes under stress. Control of transport through the NPC structure should be considered a key determinant in the adaptation of cardiac cells to metabolic challenge.

Materials and Methods

Cardiomyocytes

Cardiomyocyte cultures were prepared from hearts removed from 1- to 2-day-old rats (Harlan Sprague-Dawley, Indianapolis, Ind) after

Received January 27, 1999; accepted March 24, 1999.

From the Division of Cardiovascular Diseases and Department of Internal Medicine (C.P.-T., P.P.D., M.P., M.J., A.T.), the Department of Physical Medicine and Rehabilitation (C.P.-T.), and the Department of Pharmacology (A.M.G., R.B., F.G.P., A.T.), Mayo Clinic, Rochester, Minn. The current affiliation for Michel Puceat is Centre de Recherches de Biochimie Macromoleculaires, Montpellier, France. The current affiliation for Marisa Jaconi is Biology of Aging Laboratory, Geriatric Hospital, Geneva, Switzerland.

Correspondence to A. Terzic, Guggenheim-7, Mayo Clinic, Rochester, MN 55905. E-mail terzic.andre@mayo.edu

Circulation Research **is available at http://www.circresaha.org**

ventricles were separated and cut into 1-mm^3 pieces.[20] Tissue was digested (20 minutes, 37°C) in ADS buffer (in mmol/L: NaCl 116; HEPES 20; NaH_2PO_4 1; glucose 5.5; KCl 5.4; $MgSO_4$ 0.8; phenol red 0.6 mL/L, pH 7.35) with collagenase II (0.5 mg/mL, Worthington Biochemicals) and pancreatin (0.15 mg/mL, Life Technologies). Cell supernatant was mixed with newborn calf serum (1 mL), centrifuged (6 minutes, 1000 rpm), pellet-suspended in newborn calf serum, and incubated (37°C, 5% CO_2). After the cells were centrifuged 5 to 6 cycles to achieve full digestion, they were pooled in ADS buffer, centrifuged (6 minutes, 1000 rpm), and pellet-suspended in 8 mL of ADS. Cells were centrifuged (30 minutes, 3000 rpm) through a discontinuous 2-layer Percoll gradient. Cardiomyocytes that were present in the first layer from the bottom, were collected, suspended in ADS buffer, and centrifuged (6 minutes, 1000 rpm). Pellet was suspended in plating medium, DMEM (Gibco BRL); 17% medium 199 (Gibco); 10% horse serum (Gibco); 5% fetal bovine serum (Gibco); penicillin/streptomycin (50 U/mL, Gibco); and HEPES 20 mmol/L (pH 7.2). Cells were plated on laminin-coated coverslips and incubated in serum-containing medium (37°C, 5% CO_2).

Fluorescent Macromolecules

Histone H1, a major constituent of eukaryotic chromatin fibers, and dextrans, which lack a nuclear localization signal, are commonly used to study nuclear transport.[13,14,21,22] Dextrans of different molecular mass (3, 10, and 40 kDa) were purchased preconjugated with fluorescein isothiocyanate (FITC, Molecular Probes). H1 (Sigma Chemical Co) was labeled with FITC by use of a FITC conjugation kit (FluoroTag, Sigma). H1 (5 mg/mL) and FITC (1 mg/mL) were dissolved in 0.1 mol/L carbonate-bicarbonate buffer (pH 9.0). The FITC solution (50 μL) was added to the H1 solution (250 μL), and the mix was incubated (2 hours) with stirring. H1, conjugated with FITC, was purified by chromatography on a Sephadex G-25 column with PBS as eluent. The molar fluorescein to protein ratio (F/P) of the conjugate was calculated as $F/P = A_{495} \times C/[A_{280} - (0.35 \times A_{495})]$, where A_{495} and A_{280} are absorbances at 495 and 280 nm; and $0.35 \times A_{495}$ is the correction factor due to absorbance of FITC at 280 nm. $C = MW_{H1} \times E^{0.1\%}{}_{280}/389 \times 195$, where MW_{H1} is the molecular mass of H1 (21 kDa), 389 is the mass of FITC, 195 is the absorption of bound FITC at 495 nm (pH 13.0), and $E^{0.1\%}{}_{280}$ is the absorption at 280 nm of 1 mg/mL H1. Absorbance measurements were performed on a spectrophotometer (DU7400, Beckman). Purified fluorescein-conjugated molecules were stored in the dark (4°C). Labeled proteins were spun at 10 000g (5 minutes) before use to remove particulate matter. Neither dextrans nor H1 are cell-membrane permeable and both were microinjected into the cytosol of cardiomyocytes.

Microinjections

Fluorescent macromolecules were microinjected 48 hours after cell plating with pipettes pulled on a puller (Narishige); pipettes were made from borosilicate glass capillary (World Precision Instruments) with outer and inner diameters of 1.0 and 0.75 mm, respectively. Cells, on laminin-treated coverslips, were transferred to DMEM (37°C), which was supplemented with 0.5% BSA, 10 mmol/L HEPES (pH 7.5), and 20 mmol/L 2,3-butanedione monoxime (Sigma), used to transiently block contractions during microinjection. Microinjections were performed with the use of a nanometer-precision microinjector (Eppendorf 5242) coupled to a micromanipulator (Eppendorf 5171). Pipettes were filled with a centrifuged (10 minutes at 10 000 rpm) and prewarmed (37°C) injection buffer (in mmol/L: KCl 150, PIPES 1, EDTA 0.1, EGTA 0.025, pH 7.2) that contained fluoresceinated dextrans (5 mmol/L) or H1 (0.07 mg/mL). The injection volume was 1% to 5% of cell volume. Cells were injected in the absence or presence of agents that deplete Ca^{2+} or ATP/GTP.

Quantitation of Nuclear Transport

Cells were transferred to a chamber and superfused with (in mmol/L) NaCl 116, KCl 4, $MgCl_2$ 2, NaH_2PO_4 2, $NaHCO_3$ 4, HEPES 21, and Ca^{2+} 1 (pH 7.4, 37°C). Nuclear transport was measured with a confocal imaging system (LSM 410, Carl Zeiss) and 40× (1.3 NA) or 63× (1.4 NA) objectives were used. The thickness of the optical sections was set at 1 to 2 μm, which was necessary and sufficient to discriminate fluorescence emitted from nuclear versus nonnuclear regions. Fluorescent probes were excited (at 488 nm) with the use of an argon-krypton visible laser (Omnichrome), and the emission envelope was collected with a 510-nm-long pass dichroic beam splitter and a 515-nm-long pass emission filter. Two-dimensional confocal images (512×512 pixels) were acquired by scanning a field at 16 seconds per frame. The gain of the photomultiplier was adjusted to prevent signal saturation. Fluorescence intensity per unit area in the nucleus versus the cytosol was determined with the ANALYZE (Mayo Foundation) and NIH Image (National Institutes of Health) software. For nuclear fluorescence, the value was obtained from the total nuclear area. For cytosolic fluorescence, an area that surrounded the nucleus and equivalent to the nuclear area was used. This prevented underestimation of cytosolic fluorescence caused by thinning (<1 to 2 μm) of the cytoplasm at the edges of a cell. To confirm nuclear localization of fluoresceinated molecules, cells were optically sliced and 2-dimensional confocal images were used for 3-dimensional cellular reconstruction.

Ca^{2+} Depletion

Cardiomyocytes were loaded with the Ca^{2+} indicator fluo3 after a 30-minute (37°C) incubation with 2.5 μmol/L of the acetoxymethyl (AM) ester of fluo3 (fluo 3-AM; Molecular Probes) in plating medium.[23,24] Fluo-3–loaded cells were imaged by real-time video imaging with a confocal imaging system (LSM 410, Carl Zeiss) as described.[25] To deplete Ca^{2+} stores, cells were bathed in Ca^{2+}-free medium (with 1.1 mmol/L EGTA) and treated with Ca^{2+} ionophores ionomycin (5 μg/mL, 30 minutes) or A23187 (20 μmol/L, 10 minutes), the Ca^{2+}-ATPase inhibitor thapsigargin (2 μmol/L, 1 hour), or with the Ca^{2+} chelator BAPTA, which was used in the BAPTA-AM membrane-permeant form (10 μmol/L, 30 minutes) unless otherwise indicated. Solutions were prewarmed (37°C). Treatment with Ca^{2+}-depleting agents reduced cellular Ca^{2+} levels, as indicated by a 3- to 4-fold drop in fluo3 fluorescence, without decreasing cellular ATP/GTP levels (n=21).

ATP/GTP Depletion

Cellular ATP/GTP was depleted by inhibitors of glycolysis (2-deoxy-D-glucose; DOG) and oxidative phosphorylation (FCCP).[21] Cardiomyocytes were treated (at 37°C) with 6 mmol/L DOG and 1 μmol/L FCCP before, during, and 30 minutes after microinjection. Cells that were attached to coverslips were washed with ice-cold PBS (2 mL), and 200 μL of 0.6 mol/L $HClO_4$/1 mmol/L EDTA was layered over. Cells were detached by scraping, then they were homogenized and centrifuged (5 minutes, 12 000 rpm, 4°C). Supernatant was neutralized with 2 mol/L K_2HCO_3 and precipitate was removed by centrifugation (1 minute, 12 000 rpm, 4°C). ATP was measured in the remaining supernatant by a coupled enzyme assay in 2.5 mmol/L Tris-HCl buffer (pH 7.5), 2 mmol/L $MgCl_2$, 2 mmol/L glucose, 1 mmol/L DTT, 50 μmol/L $NADP^+$, 20 μmol/L P^1,P^5-di(adenosine-5′) pentaphosphate, 4 U/mL hexokinase, and 2 U/mL glucose-6-phosphate dehydrogenase, by use of a fluorometer with a minicell (Turner TD-700).[26] ATP and GTP were also determined by HPLC (System Gold, Beckman) with a Mono Q HR5/5 column (Pharmacia).[27] The ATP/GTP levels decreased by 80% to 90% versus in cells not treated with DOG/FCCP.

Atomic Force Microscopy

To expose intact nuclei for in situ atomic force microscopy (AFM) imaging, we used an established method that separated plasma membrane from the cytoskeleton and dissolved the plasmalemmal lipid content, which left the nucleus attached to cytoskeletal structures.[28] Cardiomyocytes were cultured in plating medium on laminin-coated 15-mm round Therminox plates (Nunc Inc). After 48 hours in culture, cells were exposed (3 minutes) to a hypotonic solution that contained the following (in mmol/L): 40 NaCl, 5.4 KCl, 0.8 $MgCl_2$, 1 NaH_2PO_4, 10 HEPES; pH 7.4. Sarcolemma was

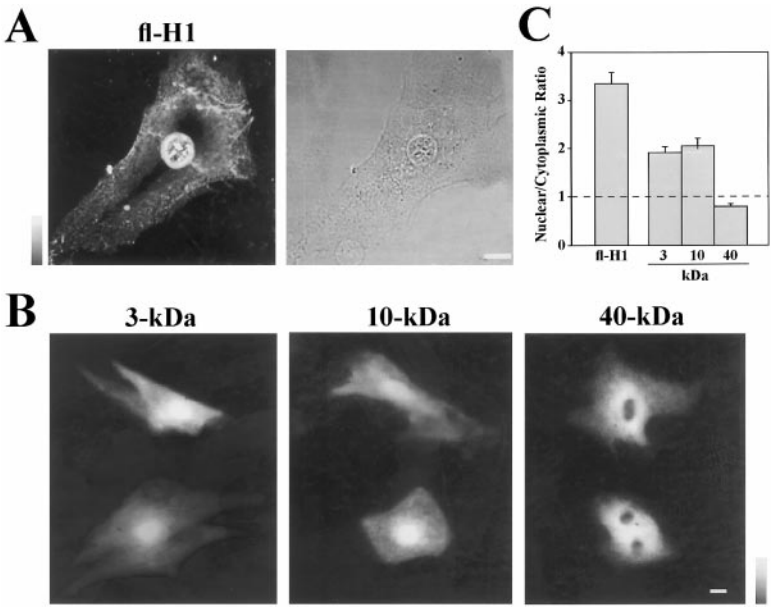

Figure 1. Nuclear transport in cardiomyocytes. A, Import of fl-H1 into the nucleus after cytosolic microinjection. Left, Confocal fluorescent image of fl-H1 in a living cardiomyocyte. Right, Confocal transmitted-light image of the same cell. Fluorescence in the left figure colocalizes with the nucleus in the right figure. B, Confocal fluorescent images of cardiomyocytes in which fluoresceinated dextrans were microinjected into cytosol. Dextrans of 3 and 10 kDa (left and middle) but not 40 kDa (right) diffused into nuclei. Horizontal bars=10 μm, and vertical bars indicate the relative fluorescent scale. C, Average nuclear-cytoplasmic ratio for fl-H1 (n=47), 3- (n=16), 10- (n=9), or 40- (n=10) kDa dextrans. A ratio $\geq$1 indicates nuclear transport, whereas a ratio $<$1 indicates exclusion of a labeled molecule from the nucleus.

removed by a 5-minute exposure to 1% Triton X-100 dissolved in (mmol/L) 75 KCl, 15 NaCl, and 20 MOPS; pH 7.4. The cytosol was washed away with (in mmol/L) 15.5 NaCl, 70 KCl, 6.5 K_2HPO_4, and 1.5 NaH_2PO_4. Sarcolemma-stripped cells, with nuclei supported by the cytoskeletal scaffold, were fixed in situ with a phosphate-buffered solution that contained 1% glutaraldehyde and 4% formaldehyde (pH 7.2) and rinsed with nanopure water and air-dried before acquisition of AFM data. We performed "contact mode AFM" in air with short, thick silicon nitride NP-S tips (spring constant: 0.58 N/m; Digital Instruments) using the Multimode AFM with a NanoScope III microscope controller (Digital Instruments). Cardiomyocytes were scanned with a large area J-type scanner ($\approx$150$\times$150 μm maximum area). The cytoplasmic surface of NPCs was scanned with a high resolution E-type scanner ($\approx$12$\times$12 μm maximum area), which allowed accurate measurements in the nanometer range. Images were collected by raster scanning across a square area at 512 pixels per line with scanning frequencies (in the *x* direction) that ranged from 2 (whole cardiomyocytes) to 15 (individual NPCs) Hz to build 512$\times$512 pixel images of the area of interest. AFM images were processed with the use of the NanoScope IIIa software (Digital Instruments). Three-dimensional AFM images were generated from topographical height information and illuminated from various angles. Each NPC was sectioned along a diameter that provided the highest point of the cytoplasmic ring and the lowest point of the pore. Four parameters were collected from each section: (1) depth of the pore (from the peak of the cytoplasmic ring to the bottom of the pore); (2) diameter of the cytosolic ring (peak to peak width); (3) overall diameter of the NPC (distance between the deepest points on either side of the NPC); and (5) height of the NPC above the surface of the nucleus (peak to the deepest point outside the NPC).

Statistics

Results are expressed as mean$\pm$SEM, and n is the number of cardiomyocytes or individual NPCs. Statistical analysis was performed by the Student *t* test. Significant difference was accepted at the $P<0.05$ level. Each experimental group was compared with its own control and prepared and analyzed simultaneously.

Results

Nuclear Import

To monitor nuclear import in living cardiomyocytes, we microinjected histone H1 (a constitutive nuclear protein) or dextrans (functionally inert molecules of different molecular size) into the cytosol. Because these molecules were fluorescein-labeled, transport into the nucleus resulted in nuclear fluorescence. Fluorescein-labeled H1 (fl-H1) transported across the nuclear envelope as seen by the high level of fluorescence in the nucleus (Figure 1A). Fluorescein-labeled dextrans of 3 and 10 kDa also entered the nucleus (Figure 1B). In contrast, 40-kDa dextrans were excluded from the nucleus with the fluorescence primarily observed in the cytosol (Figure 1B). Nuclear transport was quantified by use of the ratio of nuclear over cytosolic fluorescence; a ratio of $\geq$1 indicated nuclear transport and a ratio of $<$1 indicated exclusion of a labeled molecule from the nucleus.[13,14] For fl-H1 and 3- and 10-kDa dextrans, the ratio of nuclear over cytosolic fluorescence was $\geq$1 at 3.35$\pm$0.23 (n=47), 1.93$\pm$0.10 (n=16), and 2.06$\pm$0.14 (n=9), respectively (Figure 1C). For 40-kDa dextrans, the nuclear-cytosolic ratio was $<$1 (0.80$\pm$0.04, n=10; Figure 1C). These results show a size-restricted import of macromolecules into the nucleus of cardiomyocytes, with an upper size limit $<$40 kDa.

Ca^{2+} Regulates Nuclear Import

Maintenance of Ca^{2+} stores is required for nuclear transport.[13–16] Treatment of cardiomyocytes with BAPTA-AM (10 μmol/L), a membrane-permeant precursor to the Ca^{2+}-chelator BAPTA that buffers Ca^{2+} present throughout a cell including subcellular compartments, inhibited import of fl-H1 (Figure 2A). For fl-H1, the nuclear-cytoplasmic fluorescence ratio decreased from 3.34$\pm$0.23 (n=15) in untreated cells to 0.91$\pm$0.14 (n=15) in BAPTA-AM–treated cells (Figure 2B). Similarly, treatment of cardiomyocytes with the Ca^{2+}-pump blocker thapsigargin (2 μmol/L) in low Ca^{2+}-medium inhibited the nuclear transport of fl-H1 (Figure 2A), which resulted in a nuclear-cytoplasmic ratio of 0.71$\pm$0.08 (n=14; Figure 2B). The Ca^{2+} ionophore A23187 (20 μmol/L) in low Ca^{2+}-medium also prevented nuclear transport of fl-H1, which resulted in a nuclear-cytoplasmic ratio of 0.69$\pm$0.06 (n=8; Figure 2B).

In cardiomyocytes treated with 10 μmol/L BAPTA-AM, 2 μmol/L thapsigargin, or 20 μmol/L A23187, 10-kDa

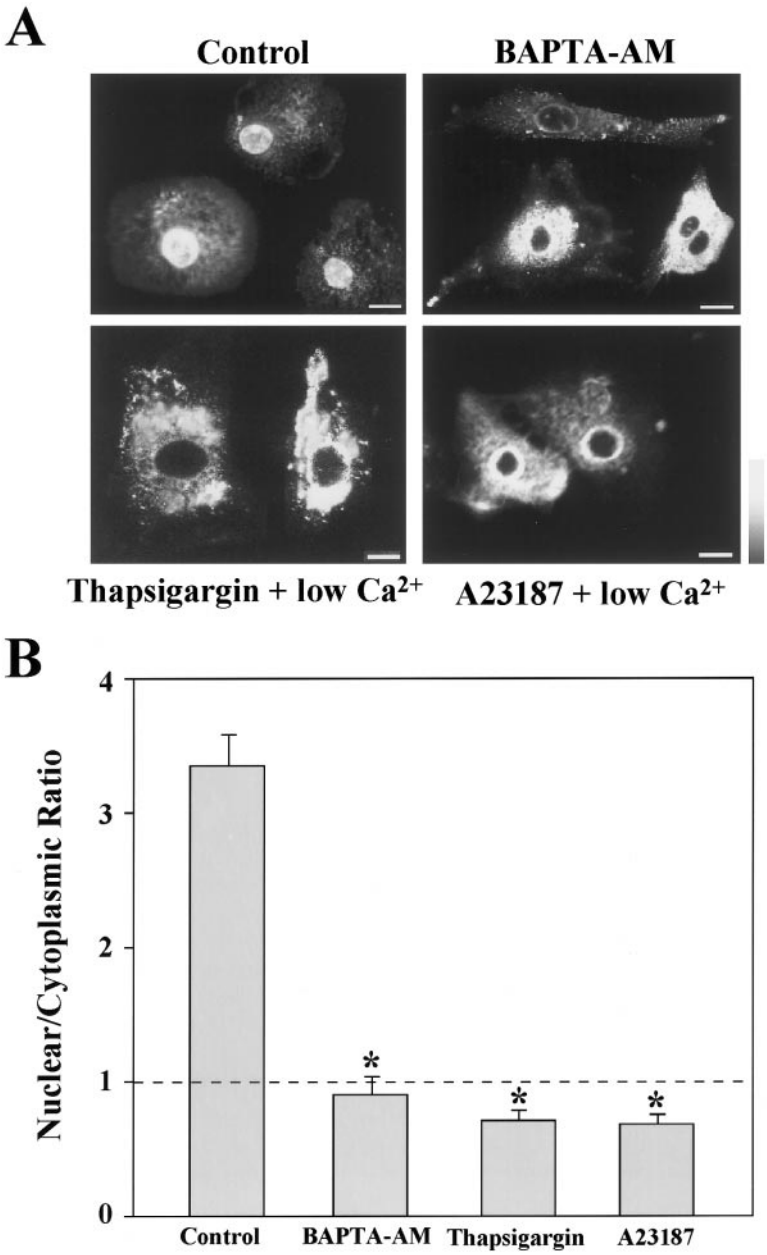

Figure 2. Ca^{2+} depletion inhibits transport of histones. Cardiomyocytes were treated without or with BAPTA-AM (10 μmol/L), thapsigargin (2 μmol/L, in low Ca^{2+} medium), or A23187 (20 μmol/L, in low Ca^{2+} medium). A, Confocal fluorescent images after microinjection of fl-H1. In contrast to controls, cardiomyocytes treated with a Ca^{2+}-depleting agent excluded fl-H1 from the nucleus. Horizontal bar=10 μm. Vertical bar indicates relative fluorescent scale. B, Nuclear-cytoplasmic ratio of fl-H1 is significantly lower (*$P<0.05$) in BAPTA-AM (n=15), thapsigargin (n=14), or A23187 (n=8) compared with cells incubated in 1 mmol/L extracellular Ca^{2+} in the absence of a Ca^{2+}-depleting drug (Control; n=15).

dextrans were excluded from the nucleus (Figure 3A). The nuclear-cytoplasmic ratio for 10-kDa dextrans was 0.74 ± 0.14 (n=5), 0.74 ± 0.03 (n=13), and 0.52 ± 0.02 (n=11), respectively (Figure 3B). In contrast, cytosolic microinjection of BAPTA itself (10 mmol/L in the pipette), which cannot cross into subcellular compartments, did not block nuclear transport of 10-kDa dextrans (Figure 3A). The nuclear-cytoplasmic ratio for 10-kDa dextrans remained >1 at 1.45 ± 0.20 (n=3; Figure 3B). The reversibility of the Ca^{2+}-dependent inhibition of nuclear transport was assessed with the Ca^{2+} ionophore ionomycin. Removal of ionomycin in the presence of extracellular Ca^{2+} allows for partial refilling of Ca^{2+} stores, including those of the endoplasmic/sarcoplasmic reticulum and associated nuclear cisterna.[13] Cardiomyocytes, in which treatment with ionomycin (5 μg/mL) in low Ca^{2+}-medium excluded 10-kDa dextran from the nucleus, partially restored nuclear transport when subsequently exposed to 1 mmol/L Ca^{2+}-containing medium with no ionomycin (Figure 3A). The nuclear-cytoplasmic ratio for 10-kDa dextrans then increased from 0.78 ± 0.05 to 1.03 ± 0.02 (n=5; $P<0.05$). Unlike large molecules, 3-kDa dextrans coupled to fluorescein transported into the nucleus regardless of the state of Ca^{2+} stores (Figure 3C and 3D). In cardiomyocytes treated with 2 μmol/L thapsigargin, the nuclear-cytoplasmic ratio for 3-kDa dextrans was similar in control (1.93 ± 0.10, n=16) and thapsigargin-treated (1.97 ± 0.18, n=10) cells. Thus, Ca^{2+} stores reversibly regulate size-dependent entry of molecules into nuclei.

ATP/GTP Differentially Regulates Nuclear Import

Certain molecules require energy for nuclear transport.[10] Depletion of ATP/GTP (with 6 mmol/L DOG and 1 μmol/L

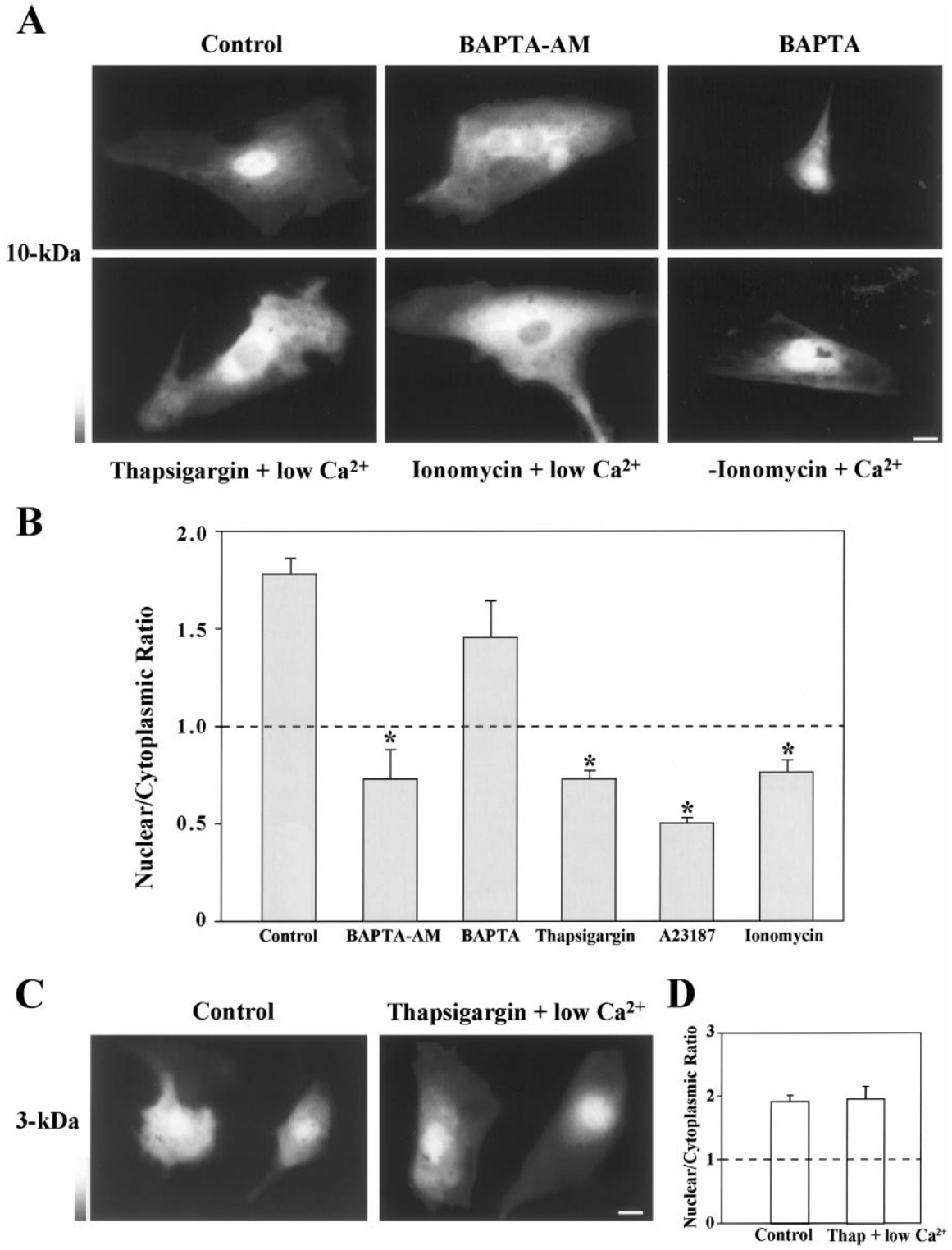

Figure 3. Depletion of Ca^{2+} inhibits nuclear transport of 10-kDa but not 3-kDa dextrans. A, Confocal fluorescent images after microinjection of fluoresceinated 10-kDa dextrans. In control cardiomyocytes (Control; 1 mmol/L extracellular Ca^{2+}), 10-kDa dextran diffused into the nucleus. Cardiomyocytes treated with ionomycin (5 μg/mL, in low Ca^{2+} medium), thapsigargin (2 μmol/L, in low Ca^{2+} medium), or BAPTA-AM (10 μmol/L) excluded 10-kDa dextrans from the nucleus. In cells microinjected with membrane-impermeant BAPTA (10 mmol/L), 10-kDa dextran diffused into the nucleus. Removal of ionomycin and the addition of 1 mmol/L $CaCl_2$ to the medium ($-$Ionomycin$+Ca^{2+}$) restored nuclear diffusion of 10-kDa dextran. Horizontal bar=10 μm. Vertical bar indicates relative fluorescent scale. B, Average nuclear-cytoplasmic ratio of fluorescein-coupled 10-kDa dextrans is significantly lower (stars indicate $P<0.05$) in BAPTA-AM– (n=5), thapsigargin– (n=13), A23187– (n=11), and ionomycin– (n=5) treated cardiomyocytes but not in BAPTA-microinjected cardiomyocytes (n=3) when compared with controls (n=11). C, Confocal fluorescent images of cardiomyocytes microinjected with fluoresceinated 3-kDa dextrans. Cells were incubated (30 minutes) in the absence or presence of thapsigargin (2 μmol/L, in low Ca^{2+} medium). In both control (1 mmol/L extracellular Ca^{2+}, left) and cells treated with thapsigargin (2 μmol/L, in low Ca^{2+} medium,

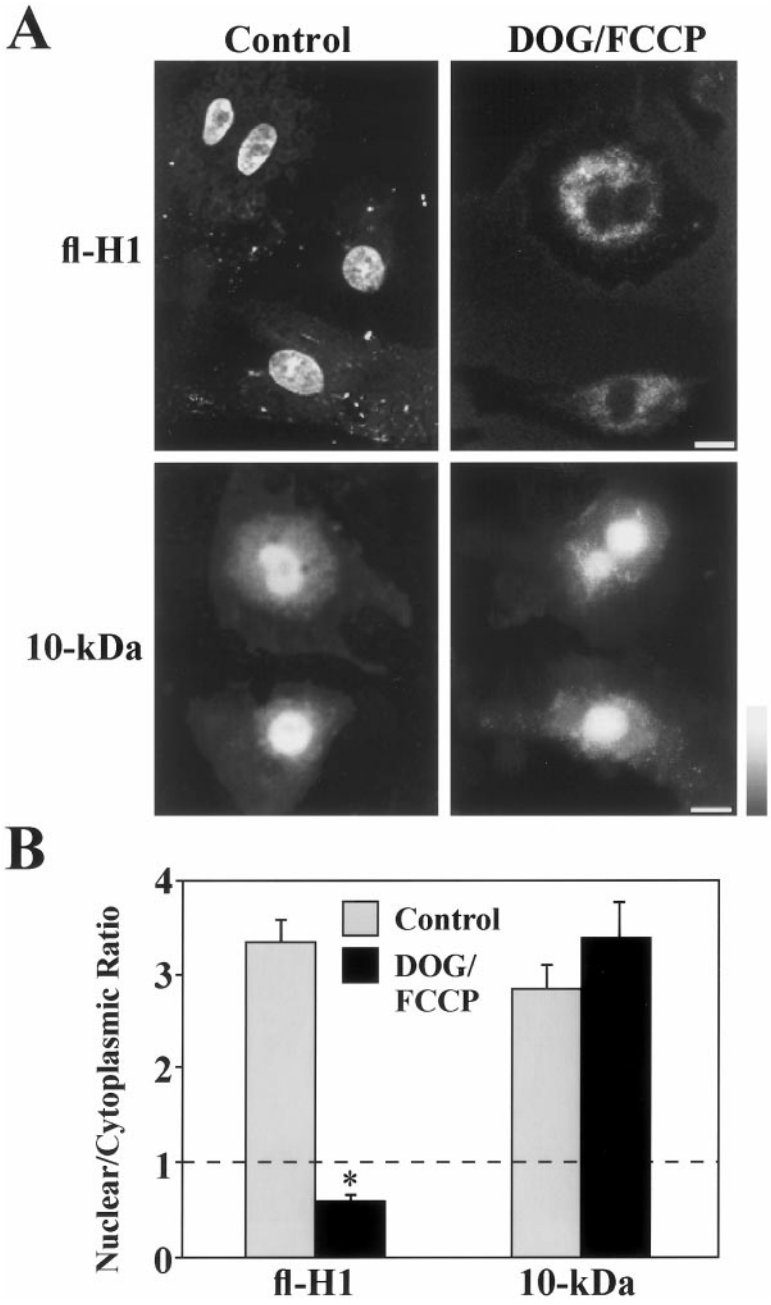

Figure 4. Depletion of ATP/GTP prevents the nuclear transport of histones but not dextrans. A (top row), Confocal fluorescent images of cardiomyocytes, with fl-H1 microinjected into the cytosol. Left, fl-H1 is imported into nuclei of control cardiomyocytes. Right, fl-H1 is excluded from nuclei of cardiomyocytes incubated for 30 minutes (37°C) in 6 mmol/L DOG and 1 μmol/L FCCP and microinjected in the presence of these ATP/GTP-depleting agents. Horizontal bar=10 μm. Vertical bar indicates relative fluorescent scale. A (bottom row), Confocal fluorescent images of cardiomyocytes microinjected with fluoresceinated 10-kDa dextrans. Dextrans diffused into the nuclei of both untreated cardiomyocytes (left) and cardiomyocytes treated (right) with 6 mmol/L DOG/1 μmol/L FCCP. Horizontal bar=10 μm. Vertical bar indicates relative fluorescent scale (white indicates highest fluorescence). B, Average nuclear-cytoplasmic ratio from cardiomyocytes microinjected with fl-H1 or 10-kDa dextrans. The ratio of fl-H1 is significantly lower (*$P<0.05$) in DOG/FCCP-treated cardiomyocytes (n=7) compared with controls (n=47). In contrast, the nuclear-cytosolic ratio for 10-kDa was >1 in both ATP/GTP-depleted (n=5) and control (n=6) cardiomyocytes ($P>0.05$).

FCCP) inhibited import of fl-H1 but did not prevent the import of 10-kDa dextrans into the nucleus (Figure 4A). In ATP/GTP-depleted cardiomyocytes, the ratio of nuclear over cytosolic fluorescence (Figure 4B) was <1 for fl-H1 (0.59±0.07; n=7) but >1 for 10-kDa dextrans (3.39±0.38; n=5). Microinjection of nonhydrolyzable ATP and GTP analogs AMPPNP and GppNHP did not rescue the import of fl-H1 into nuclei of DOG/FCCP-treated cells. In DOG/FCCP-treated cells, the nucleocytoplasmic ratio for fl-H1 was 0.43±0.05 for AMPPNP-injected (n=11) and 0.44±0.08 for GppNHP-injected (n=9) cardiomyocytes. Thus, the nuclear import of histones and dextrans in cardiomyocytes is differentially regulated by their dependence on cellular ATP/GTP pools.

right), 3-kDa dextran diffused into nuclei. Horizontal bar=10 μm. Vertical bar indicates relative fluorescent scale. D, Average nuclear-cytoplasmic ratio of fluoresceinated 3-kDa dextrans is not significantly different ($P>0.05$) in controls (n=16) versus thapsigargin (Thap) plus low Ca^{2+}-treated cardiomyocytes (n=10).

Structural Plasticity of Cardiac NPCs

To determine whether the regulation of nuclear import occurred through conformational changes in the NPC itself, nuclei were scanned by AFM in sarcolemma-stripped cardiomyocytes (n>50). The distinct morphology of cardiac nuclear envelopes showed a diffuse distribution of granular structures, which were absent from the adjacent cytoskeletal scaffold (Figure 5A). Higher resolution imaging of such granular structures revealed the toroid shape characteristic of

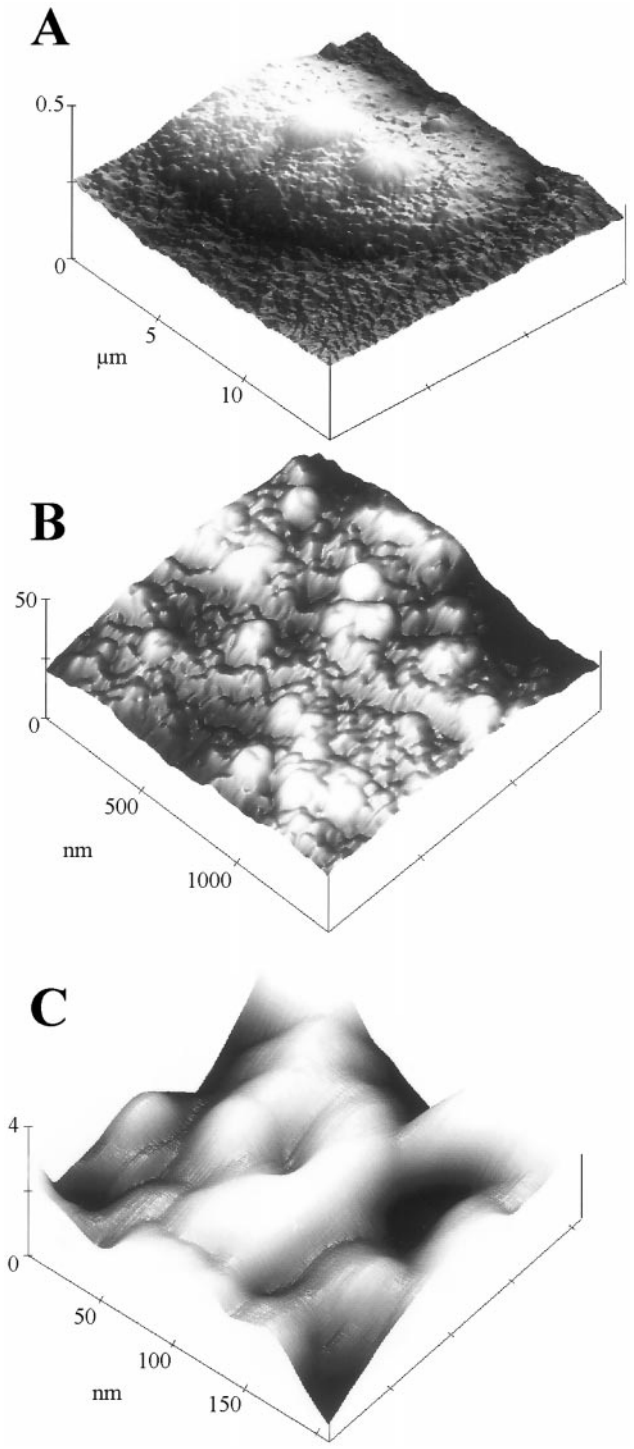

Figure 5. Three-dimensional AFM images of the cytosolic surface of cardiac nuclei. A, Cardiomyocyte stripped of sarcolemma shows the nucleus (with 2 nucleoli underneath the nuclear membrane) surrounded by remnants of cytoskeleton. B, Patch (1.5 μm^2) of the nuclear surface. Several NPCs can be seen as toroid structures embedded in the nuclear envelope. C, Individual NPC with visible central pore.

the cytoplasmic surface of NPCs (n>350 NPCs imaged and analyzed; Figure 5B). The deep central pore of an individual cardiac NPC was surrounded by a ring-like distribution of peaks (Figure 5C).

In untreated cardiomyocytes (Figure 6A), 70±4% of NPCs (n=113) displayed an open configuration of the central pore. The average pore depth of an NPC was 4.0±0.6 nm, with an NPC height of 4.2±0.6 nm (Table). In these cells, the average diameter of the cytosolic ring was 72.4±2.2 nm, whereas the NPC had an overall diameter of 164.1±6.7 nm (Table).

In cardiomyocytes in which Ca^{2+} was depleted (by 10 μmol/L BAPTA-AM), only 36±3% of the NPCs (n=152) displayed an open configuration of the central pore, a percentage significantly lower than that found in untreated cells ($P<0.05$). In the majority of NPCs from Ca^{2+}-depleted cardiomyocytes, the central channel of the nuclear pore closed in (Figure 6B). This translated into an apparent reduction in the depth of the pore to 1.2±0.1 nm (n=45; Table). The diameter of the cytosolic ring as well as the overall diameter and height of the NPC remained essentially unchanged when compared with values from untreated cells (Table).

In cardiomyocytes in which ATP/GTP was depleted (by 1 μmol/L FCCP and 6 mmol/L DOG), 40±4% of NPCs (n=146) displayed an open configuration of the central pore, which was significantly lower than that found in untreated cells ($P<0.05$). Therefore, the majority of imaged NPCs from ATP/GTP-depleted cardiomyocytes had a reduced opening of the nuclear pore (Figure 6C). The depth of the pore was 1.4±0.1 nm, with no major changes in the diameter of the cytosolic ring or in the height of the NPC (n=35; Table). However, the NPCs from ATP/GTP-depleted cells relaxed to 187.9±4.3 nm (n=35) overall diameter, a value significantly larger than the diameter of NPCs from control or Ca^{2+}-depleted cardiomyocytes ($P<0.05$; Table). Thus, we observe that depletion of Ca^{2+} or ATP/GTP reduces the probability of an open central pore and that depletion of ATP/GTP additionally induces a radial expansion of cardiac NPCs.

Discussion

This study establishes that cardiac NPCs can adopt distinct conformations that determine the outcome of macromolecular translocation across the nuclear pore. Depletion of Ca^{2+} induced closure of the nuclear pore, which indiscriminately inhibited nuclear transport of both histone H1 and 10-kDa dextrans. Depletion of cellular ATP/GTP induced a combined closure/relaxation of NPCs, which selectively inhibited nuclear transport of H1 but not dextrans. The demonstration of the structural plasticity of cardiac NPCs identifies a gating mechanism that regulates nucleocytoplasmic communication under conditions of metabolic challenge in a cardiac cell.

The NPC of mammalian cardiomyocytes displayed a structure similar to that reported for lower eukaryotic cell types.[7,8,12,15,28] A characteristic toroid structure of 150 nm in overall diameter included a multimeric cytosolic ring that surrounded a central pore. Depending on the cell type, the cutoff for nuclear import has been estimated to vary between 45 and 60 kDa.[29,30] In cardiomyocytes, we estimate a lower apparent size limit between 10 and 40 kDa. Because the excluded 40-kDa dextran has a radius of gyration of ≈5 nm, the cardiac NPC appears to have a smaller pore than that estimated in other cell types, which allows for translocation of macromolecules with a radius ≤6 nm.[10] Although the

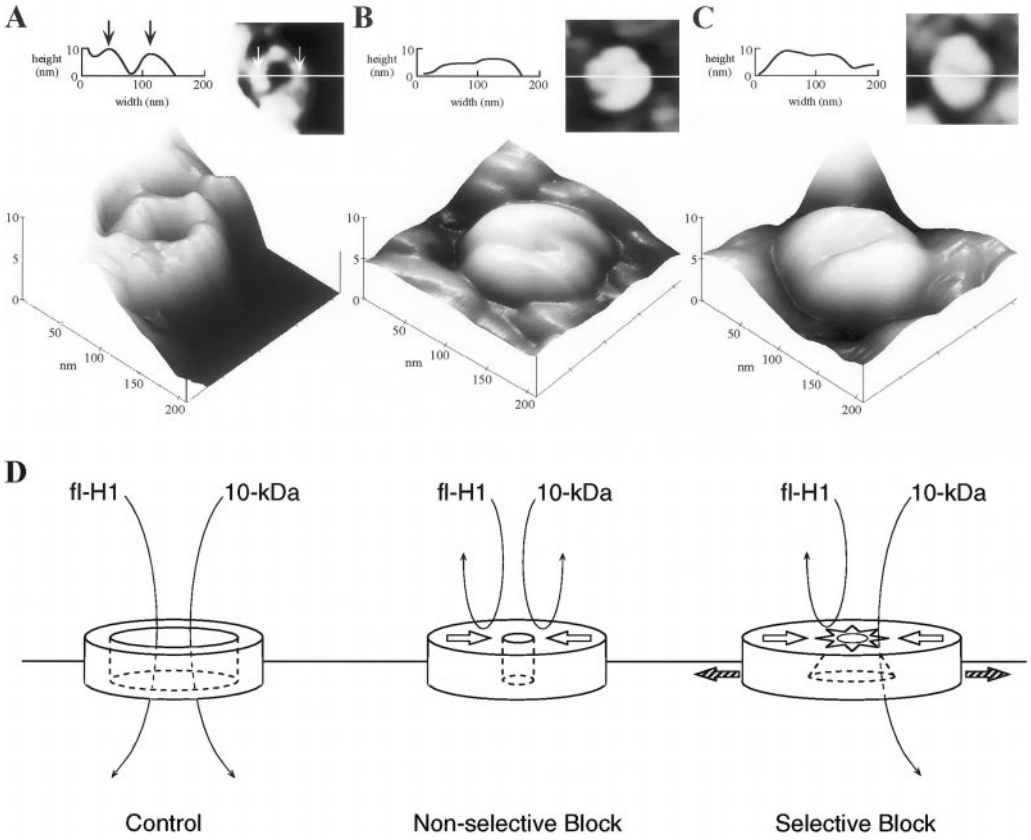

Figure 6. Structural plasticity of cardiac NPCs. High-resolution AFM images of individual NPCs from control (A), Ca^{2+}-depleted (10 μmol/L BAPTA-AM; B), and ATP/GTP-depleted (1 μmol/L FCCP/6 mmol/L DOG; C) cardiomyocytes. Although opening is observed through the center of the NPC in A, in B and C, the pore region appears to close in. The overall diameter of the NPC is larger in C than in A or B. Each 3-dimensional view is also represented by a 2-dimensional top view (upper right) and height profile (upper left). The profile is sectioned through the center of individual NPCs, as indicated by the line drawn through the center of the corresponding top view. Arrows in the height profile correspond to positions indicated by arrows on the structure of the top view. The central depression below the cytoplasmic surface of the NPC is ≈5 nm in A but diminishes to ≈1 nm in B and C. D, Model of nuclear transport regulation showing translocation of histones (fl-H1) and 10-kDa dextrans (10-kDa) under control conditions (left), nonselective block caused by Ca^{2+} depletion (middle), and selective block caused by depletion of ATP/GTP (right). Depletion of Ca^{2+} and ATP/GTP reduces the opening of the pore (open arrows), whereas depletion of ATP/GTP relaxes the complex (hatched arrows) that leads to the opening of alternate pathways for transport (starlike opening).

general structure of the NPC is conserved through evolution and its basic function is maintained,[12,19] the observed exclusion limits indicate cell type–specific differences in NPCs as conduits of nuclear transport.

Cardiac NPCs also displayed the ability to sense cellular signals. Depletion of Ca^{2+} stores induced closure of the cytosolic ring of the NPC and reduction of the apparent depth of the central pore. Repeated scanning resulted in images with identical features, which ruled out artificially generated diffuse or broad AFM images. The reduction in the height of the central pore is not due to an artifact produced by the broadening of the AFM tip because steep descents, immediately adjacent to the nuclear pore, were detectable. Instead, a change in height could indicate a vertical displacement of an

Average Dimensions of Cardiac NPCs, as Determined by AFM, Under Different Conditions of Ca^{2+} or ATP/GTP Depletion

	Pore Depth	Ring Diameter	NPC Diameter	NPC Height
Control	4.0±0.6 (69)	72.4±2.2 (35)	164.1±6.7 (30)	4.2±0.6 (65)
Ca^{2+}-depleted	1.2±0.1* (79)	71.7±2.4 (45)	159.6±2.8 (44)	3.3±0.3 (77)
ATP/GTP-depleted	1.4±0.1* (63)	71.2±2.4 (33)	187.7±4.2* (35)	5.8±0.4 (67)

Measurements are mean±SE, in nm. Numbers in parentheses indicate total number of sections through individual NPCs used in the determination of the mean. The number of NPCs analyzed was ≥35 under each condition. Two measurements, one on either side of the NPC section, were obtained for pore depth and NPC height.

*Significant difference ($P<0.05$) from control values. Cellular Ca^{2+} stores were depleted with 10 μmol/L BAPTA-AM. Cellular ATP/GTP pools were depleted with a combined treatment of 1 μmol/L FCCP and 6 mmol/L DOG.

intrinsic structure, such as a central plug, toward the cytoplasmic ring of the NPC[7,15,16] or an actual closure of the cytoplasmic ring, similar to an iris model of NPC gating.[9,31] In closed NPCs from Ca^{2+}-depleted cardiomyocytes, we observed a plug in the central pore or a twist of the cytoplasmic ring. A plug and/or twist mechanism of closing the pore, which was caused by depletion of Ca^{2+} stores, could be responsible for the observed inhibition of nuclear transport of fl-H1 and 10-kDa dextrans in cardiac cells (Figure 6D). In fact, depletion of Ca^{2+} in the contiguous reticulum/nuclear envelope may be sensed by the nucleoporin gp210, which through its putative Ca^{2+}-binding domain within the nuclear cisterna could induce conformational transitions of the NPC, including reduction in the inner diameter of the central pore.[13–16,32]

In contrast to fl-H1 and 10-kDa dextrans, 3-kDa dextrans displayed an apparent insensitivity to Ca^{2+}-depletion. This is in accord with studies in nonmammalian isolated nuclei and nuclear ghost preparations, which showed that smaller molecules ($<$ 3-kDa) freely diffuse regardless of the Ca^{2+}-filling state of the nuclear envelope.[14] This suggests that despite an apparently smaller pore, the conformational transition of cardiac NPCs, after the depletion of Ca^{2+} stores, still allows for unregulated nucleocytoplasmic distribution of smaller molecules.

Depletion of ATP/GTP inhibited nuclear import of fl-H1 without preventing the transport of 10-kDa dextrans. This is consistent with reports that transport of the constitutive nuclear protein H1 follows criteria for facilitated nuclear import, including a required nucleotide triphosphate hydrolysis.[21,22] The hypothesis that eukaryotic cells possess unfacilitated and energy-dependent facilitated nuclear transport has been established.[3] Facilitated transport is a multiple-step process, which may consume 10 nucleotide triphosphates per transport of a single molecule across the nuclear pore.[10] In this study, depletion by ≈80% to 90% of the cellular content of ATP/GTP was both sufficient and necessary to abolish nuclear transport of fl-H1. Despite a molecular mass of 21 kDa, the requirement of ATP/GTP for import indicates that H1 may form multiprotein complexes or have a large radius of gyration, either of which would prevent unfacilitated nuclear transport.[21,22]

Depletion of cellular ATP/GTP, like the depletion of Ca^{2+}, reduced the depth of the central pore and increased the number of cardiac NPCs that closed in. The mechanism that underlies the ATP/GTP-induced closing of the pore is still unknown, although it has been reported that nucleotide triphosphates may regulate the permeability of the nuclear envelope.[10,33,34] We also observed an increase in the overall diameter of the NPC in ATP/GTP-depleted cardiomyocytes. This conformational change was not observed in Ca^{2+}-depleted cells. Although methods of sample preparation could have affected the integrity of the nuclear envelope, samples for AFM were prepared in an identical manner for control, ATP/GTP-depleted, and Ca^{2+}-depleted cells. Therefore, the consistent finding of NPC expansion observed only in ATP/GTP-depleted cells is probably not the result of an artifact caused by perturbation of the envelope structure per se. The belief that the levels of nucleotide triphosphates can affect the radius of the NPC is further supported by a recent report in which the elevation of ATP levels induced constriction of the NPC complex.[35] Radial expansion could alter the inherent gating properties of NPC exposing routes peripheral to the central pore.[12] Alternative pathways at the periphery of the NPC are believed to function as diffusion channels for molecules that do not have an energy requirement for translocation across the nuclear envelope.[36] Therefore, the mechanism of selective block caused by depletion of ATP/GTP may be related in part to a combined closure/relaxation of the NPC. Although closure of the NPC would impede transport of both fl-H1 and dextrans, concomitant relaxation may expose an alternative pathway for entry of dextrans. Thus, the relaxation within the cardiac NPC combined with the closing in of the central pore may provide a structural basis for selective transport of 10-kDa dextrans despite inhibition of the nuclear import of fl-H1 in ATP/GTP-depleted cells (Figure 6D).

Thus, the current study relates conformational transitions within the cardiac NPC, induced by depletion of Ca^{2+} stores and ATP/GTP pools, to distinct patterns of nuclear import regulation. The role of Ca^{2+} depletion as a general regulator of nuclear traffic is indicated by its ability to indistinguishably block facilitated and unfacilitated transport. This is supported by the closing of the nuclear pore in Ca^{2+}-depleted cells (Figure 6D). Through the induction of a combined closure and relaxation of the nuclear pore, ATP/GTP depletion selectively allowed unfacilitated import to occur and served as a specific regulator of nuclear traffic (Figure 6D). Thus, the structural plasticity of the cardiac NPC in response to specific cellular conditions provides a mechanism for distinct regulation of nuclear import during translocation through the nuclear envelope. This depletion property renders the NPC a differential regulator of transport across the cardiac nuclear envelope.

The vigorous metabolic activity of cardiomyocytes mandates tight regulation of cellular homeostasis.[37,38] Indeed, cardiac nuclear envelopes express a high density of binding sites for IP_3.[39] This second messenger is a powerful releaser of Ca^{2+} from the nuclear cisterna,[40,41] and oscillations in cellular IP_3 have been shown to critically affect vital nuclear functions, including gene expression.[42] In this regard, neurohormones such as catecholamines, angiotensin, or endothelin as well as cellular conditions, including hypertrophy, stretch, and hypoxia, which have been associated with the generation of IP_3 and the control of gene expression in the heart, deserve to be considered as possible regulators of nuclear transport. In fact, structural changes in nuclear envelopes during elongation of heart muscle cells have already been reported.[17] Moreover, in ischemic heart disease or heart failure, disturbances in both ion and energy homeostasis accompany aberrant patterns of gene expression, which raise the possibility that altered nuclear transport contributes to progression of disease.[37,38] Therefore, identifying methods that modulate the structure of the cardiac NPC would provide a novel approach in determining regulators of nuclear transport under these conditions.

Acknowledgments

This work was supported by the American Heart Association, NIH (HL-07111), Fannie E. Rippel Foundation, Ahmanson Foundation, Miami Heart Research Institute, and the Bruce and Ruth Rappaport Program in Vascular Biology and Gene Delivery. Authors acknowledge the support by Dr G. Vassort (INSERM 323, France) and discussions with Dr E. Holmuhamedov (Mayo Clinic, Rochester, Minn).

References

1. Dingwall C, Laskey R. The nuclear membrane. *Science*. 1992;258: 942–947.
2. Nigg EA. Nucleocytoplasmic transport: signals, mechanism and regulation. *Nature*. 1997;386:779–787.
3. Gorlich D, Mattaj IW. Nucleocytoplasmic transport. *Science* 1996;271: 1513–1518.
4. Pante N, Aebi U. Sequential binding of import ligands to distinct nucleopore regions during their nuclear import. *Science*. 1996;273: 1729–1732.
5. Pemberton L, Blobel G, Rosenblum J. Transport routes through the nuclear pore complex. *Curr Opin Cell Biol*. 1998;10:392–399.
6. Ohno M, Fornerod M, Mattaj IW. Nucleocytoplasmic transport: the last 200 nanometers. *Cell*. 1998;92:327–336.
7. Akey CW, Radermacher M. Architecture of the *Xenopus* nuclear pore complex revealed by three-dimensional cryo-electron microscopy. *J Cell Biol*. 1993;122:1–19.
8. Pante N, Aebi U. Towards understanding the 3-D structure of the nuclear pore complex at the molecular level. *Curr Opin Struct Biol*. 1996;4: 187–196.
9. Akey CW. Interactions and structure of the nuclear pore complex revealed by cryo-electron microscopy. *J Cell Biol*. 1989;109:955–970.
10. Hanover JA. The nuclear pore at the crossroads. *FASEB J*. 1992;4: 187–196.
11. Pante N, Aebi U. The nuclear pore complex. *J Cell Biol*. 1993;122: 977–984.
12. Yang Q, Rout MP, Akey CW. Three-dimensional architecture of the isolated yeast nuclear pore complex: functional and evolutionary implications. *Mol Cell*. 1998;1:223–234.
13. Greber UF, Gerace L. Depletion of calcium from the lumen of endoplasmic reticulum reversibly inhibits passive diffusion and signal-mediated transport into the nucleus. *J Cell Biol*. 1995;128:5–14.
14. Stehno-Bittel L, Perez-Terzic C, Clapham DE. Diffusion across the nuclear envelope inhibited by depletion of the nuclear calcium store. *Science*. 1995;270:1835–1838.
15. Perez-Terzic C, Pyle J, Jaconi M, Stehno-Bittel L, Clapham D. Conformational states of the nuclear pore complex induced by depletion of nuclear Ca^{2+} stores. *Science*. 1996;273:1875–1877.
16. Akey CW. Structural plasticity of the nuclear pore complex. *J Mol Biol*. 1995;248:273–293.
17. Bloom S. Structural changes in nuclear envelopes during elongation of heart muscle cells. *J Cell Biol*. 1970;44:218–223.
18. Sweitzer TD, Hanover JA. Calmodulin activates nuclear protein import: a link between signal transduction and nuclear transport. *Proc Natl Acad Sci U S A*. 1996;93:14574–14579.
19. Corbett AH, Silver PA. Nucleocytoplasmic transport of macromolecules. *Microbiol Mol Biol Rev*. 1997;61:193–211.
20. Puceat M, Hilal-Dandan R, Strulovici B, Brunton LL, Brown JH. Differential regulation of protein kinase C isoforms in isolated neonatal and adult rat cardiomyocytes. *J Biol Chem*. 1994;269:16938–16944.
21. Breeuwer M, Goldfarb DS. Facilitated nuclear transport of histone H1 and other small nucleophilic proteins. *Cell*. 1990;60:999–1008.
22. Kurz M, Doenecke D, Albig W. Nuclear transport of H1 histones meets the criteria of a nuclear localization signal-mediated process. *J Cell Biochem*. 1997;64:573–578.
23. Jovanovic A, Jovanovic S, Lorenz E, Terzic A. Recombinant cardiac ATP-sensitive K^+ channel subunits confer resistance to chemical hypoxia-reoxygenation injury. *Circulation*. 1998;98:1548–1555.
24. Perez-Terzic C, Stehno-Bittel L, Clapham D. Nucleoplasmic and cytoplasmic differences in the fluorescence properties of the calcium indicator Fluo-3. *Cell Calcium*. 1997;21:275–282.
25. Perez-Terzic C, Jaconi M, Stehno-Bittel L. Measurement of intracellular calcium using confocal microscopy. *Methods Mol Biol*. 1999;114:75–91.
26. Dzeja PP, Zeleznikar RJ, Goldberg ND. Suppression of creatine kinase-catalyzed phosphotransfer results in increased phosphoryl transfer by adenylate kinase in intact skeletal muscle. *J Biol Chem*. 1996;271: 12847–12851.
27. Olson LK, Schroeder W, Robertson RP, Goldberg ND, Walseth TF. Suppression of adenylate kinase catalyzed phosphotransfer precedes and is associated with glucose- induced insulin secretion in intact HIT-T15 cells. *J Biol Chem*. 1996;271:16544–16552.
28. Oberleithner H, Brinckmann E, Schwab A, Krohne G. Imaging nuclear pores of aldosterone-sensitive kidney cells by atomic force microscopy. *Proc Natl Acad Sci U S A*. 1994;91:9784–9788.
29. Gerace L, Burke B. Functional organization of the nuclear envelope. *Annu Rev Cell Biol*. 1988;4:335–374.
30. Peters R. Fluorescence microphotolysis to measure nucleocytoplasmic transport and intracellular mobility. *Biochim Biophys Acta*. 1986;864: 305–359.
31. Akey CW. Visualization of transport-related configurations of the nuclear pore transporter. *Biophys J*. 1990;58:341–355.
32. Perez-Terzic C, Jaconi M, Clapham DE. Nuclear calcium and the regulation of the nuclear pore complex. *Bioessays*. 1997;19:787–792.
33. Assandri R, Mazzanti M. Ionic permeability on isolated mouse liver nuclei: influence of ATP and Ca^{2+}. *J Membr Biol*. 1997;157:301–319.
34. Moore MS. Ran and nuclear transport. *J Biol Chem*. 1998;273: 22857–22860.
35. Rakowska A, Danker T, Schneider S, Oberleithner H. ATP-induced shape change of nuclear pores visualized with the atomic force microscope. *J Membr Biol*. 1998;163:129–136.
36. Hinshaw JE, Carragher BO, Milligan RA. Architecture and design of the nuclear pore complex. *Cell*. 1992;69:1133–1141.
37. Cohn JN, Bristow MR, Chien KR, Colucci WS, Frazier OH, Leinwand LA, Lorell BH, Moss AJ, Sonnenblick EH, Walsh RA, Mockrin SC, Reinlib L. Report of the National Heart, Lung, and Blood Institute Special Emphasis Panel on Heart Failure Research. *Circulation*. 1997;95: 766–770.
38. Kloner RA, Bolli R, Marban E, Reinlib L, Braunwald E. Medical and cellular implications of stunning, hibernation, and preconditioning. *Circulation*. 1998;97:1848–1867.
39. Guihard G, Proteau S, Rousseau E. Does the nuclear envelope contain two types of ligand-gated Ca^{2+} release channels? *FEBS Lett*. 1997;414: 89–94.
40. Gerasimenko OV, Gerasimenko JV, Tepikin AV, Petersen OH. ATP-dependent accumulation and inositol trisphosphate- or cyclic ADP-ribose-mediated release of Ca^{2+} from the nuclear envelope. *Cell*. 1995; 80:439–444.
41. Stehno-Bittel L, Luckhoff A, Clapham DE. Calcium release from the nucleus by $InsP_3$ receptor channels. *Neuron*. 1995;14:163–167.
42. Li W, Llopis J, Whitney M, Zlokarnik G, Tsien RY. Cell-permeant caged $InsP_3$ ester shows that Ca^{2+} spike frequency can optimize gene expression. *Nature*. 1998;392:936–941.